CORTEX XXX (2012) 1–17

Available online at www.sciencedirect.com

SciVerse ScienceDirect

Journal homepage: www.elsevier.com/locate/cortex

Special issue: Research report

Subdivision of the occipital lobes: An anatomical and functional MRI connectivity study

Michel Thiebaut de Schotten [a,b,c,d,*], *Marika Urbanski* [b,c,f], *Romain Valabregue* [b,c,d,e], *Dimitri J. Bayle* [c] *and Emmanuelle Volle* [b,c]

[a] *Natbrainlab, Department of Forensic and Neurodevelopmental Sciences, Institute of Psychiatry, King's College London, London, UK*
[b] *Université Pierre et Marie Curie-Paris 6, Centre de Recherche de l'Institut du Cerveau et de la Moelle épinière (CRICM), UMRS 975, Paris, France*
[c] *Inserm, U 975, Paris, France*
[d] *CNRS, UMR 7225, Paris, France*
[e] *Centre de Neuroimagerie de Recherche CENIR, Groupe Hospitalier Pitié-Salpêtrière, Paris, France*
[e] *Service de Médecine et de Réadaptation, Hôpitaux de Saint-Maurice, Saint-Maurice, France*

ARTICLE INFO

Article history:
Received 28 May 2012
Reviewed 3 July 2012
Revised 24 September 2012
Accepted 6 December 2012
Published online xxx

Keywords:
Anatomy
Occipital subdivision
Diffusion weighted imaging
Tractography
fMRI
Functional connectivity
Resting state
White matter

ABSTRACT

Exploring brain connectivity is fundamental to understanding the functional architecture of the cortex. In our study we employed tractography-based parcellation, combined with the principal component analysis statistical framework, to divide the occipital lobes into seven areas in a group of eighteen healthy participants. Tractography-based parcellation is a method based on diffusion imaging tractography, which segregates the living human brain into distinctive areas showing sharp differences in their anatomical connectivity. The results were compared to covarying functional networks involving distinct areas within the occipital lobes, that we obtained using resting state functional magnetic resonance imaging (fMRI), as well as to other existing subdivisions of the occipital lobes. Our results showed similarities with functional imaging data in healthy controls and cognitive profiles in brain-damaged patients, although several differences with cytoarchitectonic, myelogenetic, myeloarchitectonic and functional maps were reported. While the similarities are encouraging, the potential validity and limitations of the differences observed are discussed. Taken together these results suggest that tractography-based parcellation may provide a new promising anatomical subdivision of the living human brain based on its anatomical connectivity, which may benefit the understanding of clinical-neuroanatomical dissociations and functional neuroimaging results.

1. Introduction

During the course of the last 50 years, many developments in our knowledge of the human's occipital lobe stem from the monkey's occipital lobe having been segregated into several sharply defined subdivisions of visually responsive cortex using direct electrical recording (Felleman and Van Essen, 1991; Hubel and Wiesel, 1962; Van Essen, 2003; Van Essen

* *Corresponding author*. CRICM-UMRS975/UMR7225, 47 Bd de l'Hôpital, 75651 Paris Cedex 13, France.
E-mail address: michel.thiebaut@gmail.com (M. Thiebaut de Schotten).

0010-9452/$ – see front matter © 2012 Elsevier Ltd. All rights reserved.
http://dx.doi.org/10.1016/j.cortex.2012.12.007

and Maunsell, 1983; Zilles and Clarke, 1997). Most of these subdivisions show clear differences in their anatomical features, and given that electrical recording is very difficult in the living human brain, anatomists used these anatomical features as landmarks to parcellate the occipital lobes in humans. These anatomical landmarks included, for instance, the visible variation in the neuronal pattern of the six cortical layers (i.e., cytoarchitectonic) (Amunts et al., 2000; Brodmann, 1909; Campbell, 1905; Von Economo and Koskinas, 1925; Zilles et al., 1986), the density of myelinated fibres (i.e., myeloarchitectonic) (Smith, 1907; Vogt and Vogt, 1919; Zilles and Schleicher, 1993), the progressive myelination during maturation of the human brain (Flechsig, 1920) or how sub-regions of the occipital lobe are connected with the rest of the brain (Burkhalter and Bernardo, 1989; Clarke, 1993; Clarke and Miklossy, 1990). Two common factors underlying these subdivisions of the living human brain are that they employ post-mortem techniques and that they are difficult to translate into in-vivo specimens due to inter-individual variability. Alternative methods to subdivide the human living brain into distinct areas sharing close anatomical features are therefore required to allow us to associate variability in these subdivisions with healthy and pathological conditions.

Exploring brain connectivity is a fundamental approach to study the functional architecture of the cortex (Mesulam, 2005). For example, although neurons from visual and auditory cortices share similar anatomy and organisation, they support different functions, and show clear differences in their anatomical connectivity with the rest of the brain. These differences in connectivity, may explain their functional specificity (in humans see Catani et al., 2003, 2005; ffytche et al., 2010; in monkeys see Petrides and Pandya, 2009; Yeterian and Pandya, 2010). This suggests that one of the best methods to studying the functional specialisation of specific brain regions is to examine the nature of the input and output of that region (Van Essen and Maunsell, 1983).

The study of both anatomical and functional connectivity in the living human brain has shown a considerable expansion in the last decade thanks to the development of diffusion-weighted imaging (DWI) tractography techniques (Basser et al., 2000; Dell'acqua and Catani, 2012; Dell'acqua et al., 2010; Jones, 2008) as well as functional magnetic resonance imaging (fMRI) connectivity methods (Deco et al., 2011; Fox and Raichle, 2007; Greicius et al., 2003; Mantini et al., 2007). Tractography studies reconstruct white matter anatomical features in the living human brain, which show similarities with those reported in post-mortem animal tracing studies (Dauguet et al., 2007; Rilling et al., 2008; Thiebaut de Schotten et al., 2011a, 2012) and in human brain dissections (Catani et al., 2012; Lawes et al., 2008; Thiebaut de Schotten et al., 2011b). Resting state fMRI (rsfMRI) connectivity studies identify brain areas with similar dynamics of blood/oxygen level (BOLD) signal changes, i.e., covarying functional networks. Hence, rsfMRI connectivity has been employed to decompose data into a set of distinct spatial maps, each with its own time course (Kiviniemi et al., 2003). Recently, independent component analysis has been optimised to extract the major covarying networks in the resting brain, as imaged with rsfMRI (Beckmann et al., 2005). These networks are very consistent across subjects (Damoiseaux et al., 2006) and closely correspond to major task-related networks as identified using standard fMRI paradigms (Smith et al., 2009). However, it is unknown whether all these functional connectivity networks reflect specific anatomical features. Some rsfMRI connectivity studies showed patterns of connectivity comparable to those revealed with anatomical tractography (Greicius et al., 2009; Honey et al., 2009; Skudlarski et al., 2008), but functional and anatomical connectivities are not necessarily similar. For example, rsfMRI connectivity may vary according to the functional state of the measured brain (Fox et al., 2006; Ginestet and Simmons, 2010; Hampson et al., 2006; He et al., 2007; McAvoy et al., 2008; Seeley et al., 2007; Zhou et al., 2011). Hence, anatomical connectivity and functional connectivity are not strictly equivalent but rather complementary (Deco et al., 2011; Honey et al., 2009).

Tractography can also be used to divide a brain area into sub-regions defined by a similar anatomical connectivity pattern. Tractography-based parcellation has been employed to segregate functionally different but anatomically adjacent areas, such as the supplementary motor area (SMA) and the pre-SMA (Johansen-Berg et al., 2004) or Brodmann areas (BA) 44 and 45 (Anwander et al., 2007), because they exhibit sharp changes in their connectivity. These results suggest a close alignment between tractography-based parcellation of the living human brain and functional and cytoarchitectonic regions (Jbabdi and Behrens, 2012). More recently other authors employed tractography-based parcellation to describe a new in-vivo parcellation of the inferior parietal cortex into five regions (Mars et al., 2011) that correspond to recent post-mortem cytoarchitectonic atlases (Caspers et al., 2008, 2006). However, the statistical framework used for tractography-based parcellation is limited by the need to determine *a priori* the number of sub-regions to expect from the parcellation, which relies on the experimenter's subjectivity. This is a crucial issue in cases of blind parcellation approaches that aim to detect functional sub-units without strong prior hypotheses (Jbabdi et al., 2009).

In the present study, we employed a principal component analysis, which divided the occipital lobe into several regions that showed a different pattern of anatomical connectivity as revealed by probabilistic tractography, without determining *a priori* the number of sub-regions. We report seven distinct sub-regions in each occipital lobe, as well as their hemispheric asymmetries. Results are compared to rsfMRI covarying networks obtained in the same subjects, and also to standard myeloarchitectonic (Smith, 1907), cytoarchitectonic (Caspers et al., 2012, 2008, 2006; Kujovic et al., 2012; Rottschy et al., 2007), myelogenetic (Flechsig, 1920) maps obtained from post-mortem dissections, functional maps transposed from monkey to humans (Van Essen, 2003), fMRI results and clinical-anatomical conclusions built from neuropsychological studies.

2. Methods

2.1. Participants and MRI acquisitions

The study was approved by the local Ethics Committee. Eighteen right-handed participants (10 males and eight

Please cite this article in press as: Thiebaut de Schotten M, et al., Subdivision of the occipital lobes: An anatomical and functional MRI connectivity study, Cortex (2012), http://dx.doi.org/10.1016/j.cortex.2012.12.007

females) gave informed consent to participate in this study. The average age of participants was 37.33 (±13.66 years).

A total of 70 near-axial slices were acquired on a Siemens 3 T VERIO TIM system equipped with a 32-channel head coil. We used an acquisition sequence fully optimised for tractography of DWI, which provided isotropic (2 × 2 × 2 mm) resolution and coverage of the whole head. The acquisition was peripherally-gated to the cardiac cycle (Conturo et al., 1995; Jones et al., 2002; Turner et al., 1990) with an echo time (TE) = 85 msec. We used a repetition time (TR) equivalent to 24 RR intervals assuming that spins would have fully relaxed before the repetition. At each slice location, six images were acquired with no diffusion gradient applied. Additionally, 60 diffusion-weighted images were acquired, in which gradient directions were uniformly distributed in space. The diffusion weighting was equal to a *b*-value of 1500 sec mm^{-2}.

The same participants underwent a fMRI session of resting state. During the resting state session, participants were instructed to relax, keep their eyes closed but to avoid falling asleep. Functional images were obtained using T2-weighted echo-planar imaging (EPI) with blood oxygenation level-dependent (BOLD) contrast using SENSE imaging. EPIs (TR/TE = 3000/26 msec) comprised 32 axial slices acquired continuously in ascending order covering the entire cerebrum (voxel size = 2 × 2 × 3 mm^3).

An axial three-dimensional (3D) magnetization prepared RApid gradient echo (MPRAGE) dataset covering the whole head was also acquired for each participant (176 slices, voxel resolution = 1 × 1 × 1 mm, TE = 3 msec, TR = 2300 msec, flip angle = 9°).

2.2. *Occipital lobe mask*

For the left and the right hemispheres, an occipital lobe mask was drawn on the Colin27 template (Holmes et al., 1998) provided in MRIcron (www.mccauslandcenter.sc.edu/mricro/mricron/) using surface anatomical landmarks.

The temporal and occipital lobes are separated by an arbitrary line between the dorsal tip of the parieto-occipital sulcus and the pre-occipital notch. We overestimated the lateral border of the occipital lobe including the most posterior part of the angular gyrus and part of the inferior and middle temporal gyri in the mask. This choice was made in order to avoid artificial borders in the parcellation. For the medial surface, the parieto-occipital sulcus was used to divide the parietal from the occipital lobe, and ventrally an arbitrary line from the pre-occipital notch to the lower tip of the parieto-occipital sulcus was used to separate the occipital and temporal lobes (Catani and Thiebaut de Schotten, 2012).

The left and the right occipital lobes were registered to the individual MPRAGE datasets using Advance Normalization Tools (ANTs, http://www.picsl.upenn.edu/ANTS/), which combine affine with diffeomorphic deformations (Avants et al., 2008; Klein et al., 2009).

2.3. *DWI tractography*

Diffusion-weighted datasets were corrected for head motion and eddy current distortions using affine registration to a non-diffusion-weighted reference volume (Jenkinson and Smith, 2001) as implemented in the FMRIB Software Library (FSL) software package (http://www.fmrib.ox.ac.uk/fsl/) (Smith et al., 2004). White matter orientation estimation was performed with a Bayesian Estimation of Diffusion Parameters Obtained using Sampling Techniques (bedpostx, Behrens et al., 2007) modelling in our study for up to two populations of fibres crossing within the same voxel.

A tractography algorithm based on a probabilistic approach (Behrens et al., 2007) (20,000 samples, step length .5 mm, curvature threshold of .2) was used to propagate streamlines from 'seed' to 'target' regions of interest (ROIs) (http://brainvisa.info) situated in the white matter that was the closest to the grey matter. Within the white matter, water molecules diffuse more freely along axons than across them (Moseley et al., 1990), making it possible to obtain in-vivo estimates of white matter fibre orientation by measuring the diffusivity of water molecules along different directions (Basser et al., 1994, 2000; Basser and Pierpaoli, 1996). Alternatively, water molecules diffuse more randomly within the grey matter because of its more complex organisation, which includes neuronal cell bodies, glial cells, capillaries, dendrites and axons. This uncertainty often leads to erroneous estimates of white matter fibre orientation and may flaw the tractography. Therefore, we created thin white matter ROIs, which were laid just below the grey matter ribbon. These ROIs were obtained using the intersection between white matter and the smoothed (2 mm full width at half maximum isotropic Gaussian kernel and using a lower threshold of .5) grey matter tissue types originally segmented with Oxford Centre for functional MRI of the Brain (FMRIBs) Automated Segmentation Tool (FAST) and applied to the MPRAGE dataset (Zhang et al., 2001). The result was then segmented into small ROIs of about 6 mm^2 (and 1 voxel thick) covering the entire white matter surface beneath the grey matter ribbon. In order to minimise the amount of variables representing false positives due to complex configuration such as kissing and fanning connections, additional ROIs were defined manually for the corpus callosum, the thalamus and basal ganglia territories and used as target ROIs for the parcellation (Behrens et al., 2003; Catani and Thiebaut de Schotten, 2008).

The skull was extracted from the MPRAGE dataset using Brain Extraction Tool (BET) provided in FMRIB Software Library. The skull-stripped MPRAGE dataset and the ROIs were then registered to the B0 volume of the diffusion-weighted dataset using affine (FMRIB's Linear Image Registration Tool – FLIRT) deformation provided in FSL.

From each ROI in the left and right occipital masks, we seeded the tractography and recorded the proportion of streamlines that passed through each of the other ROIs as a surrogate of the 'probability of connection' to that zone (Fig. 1a–c). This 'probability of connection' was corrected for size and the distance of the target using the following formula: [(number of tracks connecting the target ROI)/(number of voxel of the target ROI)] × (length of the tracks).

For each participant, a 'connectivity' matrix between occipital ROIs (seeds) and each other ROIs of the ipsilateral hemisphere (targets) was derived from the data of the probabilistic tractography (no threshold) (Johansen-Berg et al., 2004). This matrix consisted of columns that indicated each occipital ROI, and rows that represented each ipsilateral hemisphere ROI.

Please cite this article in press as: Thiebaut de Schotten M, et al., Subdivision of the occipital lobes: An anatomical and functional MRI connectivity study, Cortex (2012), http://dx.doi.org/10.1016/j.cortex.2012.12.007

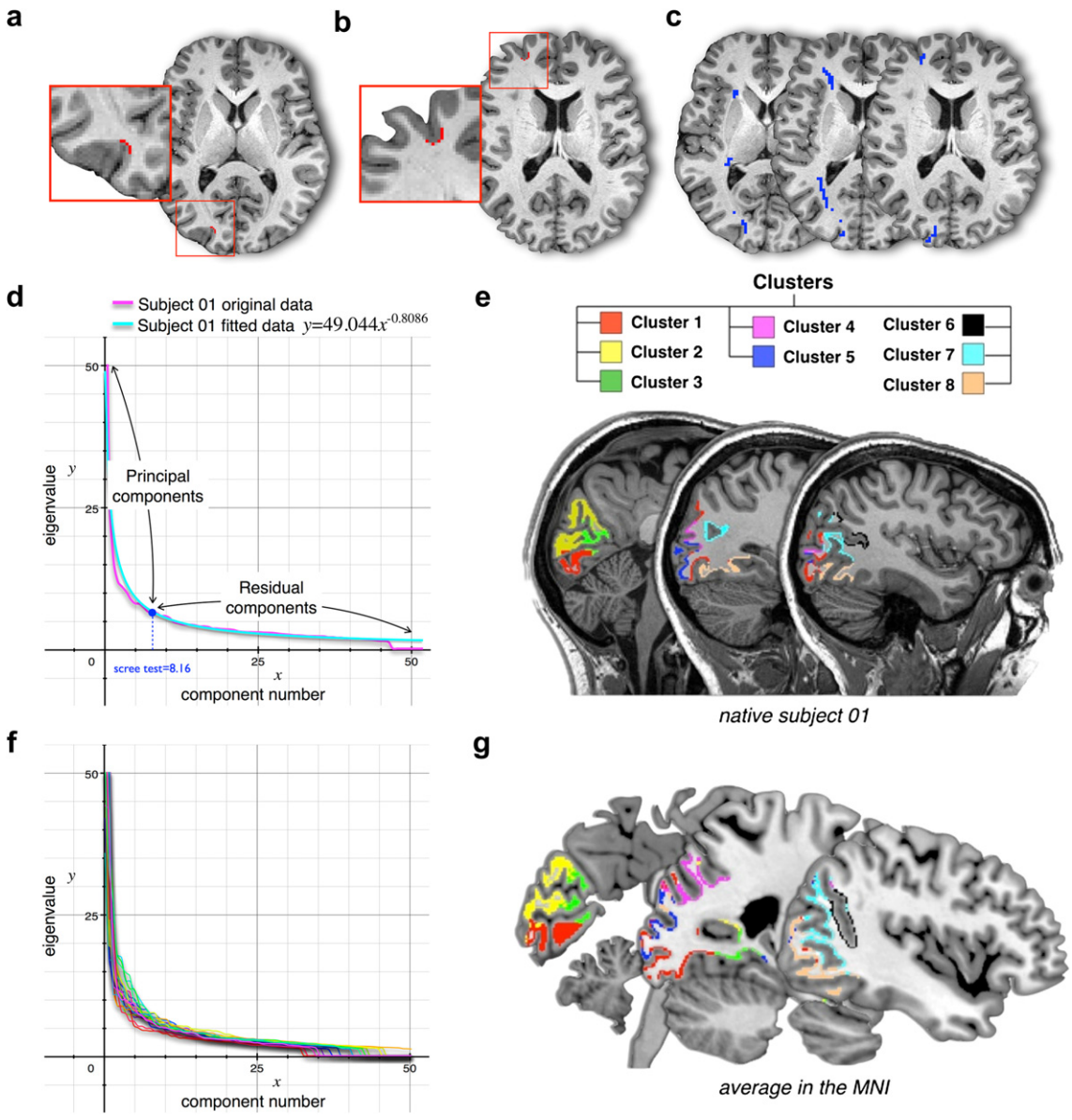

Fig. 1 – Individual and group parcellation of the left occipital lobe. (a) Example of a seed ROI for the tractography. (b) Example of a target ROI for the tractography. (c) Example of the probabilistic tractography seeded from (a) to the target (b). (d) Graph of the principal components (*x*) according to their eigenvalue sizes (*y*) for one representative subject. Original data is represented in purple and fitted data in cyan. (e) Cluster extracted from the second principal component analysis in one representative subject. (f) Graph of the principal components (*x*) according to their eigenvalue sizes (*y*) for all subjects. Different colours are used for each subject. (g) Group parcellation of the left occipital lobe obtained from averaging the result of the 18 participants.

2.4. *Tractography-based parcellation*

Statistical analysis was performed using SPSS software (SPSS, Chicago, IL). Each value of the 'connectivity' matrix obtained from the tractography was converted into z-scores and entered into a first principal component analysis using a covariance matrix and quartimax rotation (with a maximum of 50 iterations for convergence) in order to estimate the number of principal components to extract for each subject (Fig. 1d). We plotted the components in order, according to their eigenvalue (*y*) and applied a scree test to separate the principal from residual components (Fig. 1d) (Cattell, 1966). The data was fitted to a power curve and the inflexion point was extracted using a homemade routine written in Matlab 7.8 (http://www.matwork.com). In average, 8.2 (±.56) and eight (±.44) factors were obtained for the left and the right hemispheres respectively.

A second principal component analysis was performed similarly, this time with a fixed number of eight factors to extract. The result was used to group together ROIs (registered with MPRAGE and diffusion datasets) of the occipital lobes in eight clusters, which corresponded to the eight factors

Please cite this article in press as: Thiebaut de Schotten M, et al., Subdivision of the occipital lobes: An anatomical and functional MRI connectivity study, Cortex (2012), http://dx.doi.org/10.1016/j.cortex.2012.12.007

extracted from the second principal component analysis (Fig. 1e).

For each lobe, the eight clusters registered with the MPRAGE dataset were registered to the Colin27 template using the inverse of the affine and diffeomorphic deformations estimated with ANTs to register the left and the right occipital lobes with the individual MRrage datasets. The individual registered clusters were overlapped into eight average clusters. These average clusters were gathered in a single file with the command find_the_biggest in FSL, which displayed clusters with the highest probability of overlap (Figs. 1g and 2a). Display of axial brain slices was performed using MRIcron (http://www.mccauslandcenter.sc.edu/mricro/mricron). 3D rendering of the brains were calculated using the T1 pipeline in BrainVISA. The overall visualisation and screenshots were performed using the software anatomist (http://brainvisa.info).

2.5. Pattern of 'anatomical connectivity'

In this section, we challenged the validity of our method of parcellation by propagating the tractography from the eight clusters revealed by individual parcellation. Our analysis concentrated on voxels strictly within the occipital lobe, using an arbitrary line between the dorsal tip of the parieto-occipital sulcus and the pre-occipital notch as lateral border. This choice was made in order to consider only the 'anatomical connectivity' emerging from the occipital lobe. For each lobe, the eight clusters registered with the diffusion dataset were used as a seed to propagate the tractography and create maps of 'anatomical connectivity' for each of these regions. Each of the 'anatomical connectivity' maps was registered to the Colin27 template using the inverse of the affine and diffeomorphic deformations to register the left and the right occipital lobes with the individual MRrage datasets. The average registered maps of 'anatomical connectivity' were overlapped and displayed in Figs. 3 and 4 for each of the eight clusters and we choose a lower threshold of 20,000 (corresponding to the 20,000 individual pathways or samples that are drawn through the probability distributions on principle fibre direction). The upper threshold was set at 500,000 subjectively in order to facilitate reading of the figure.

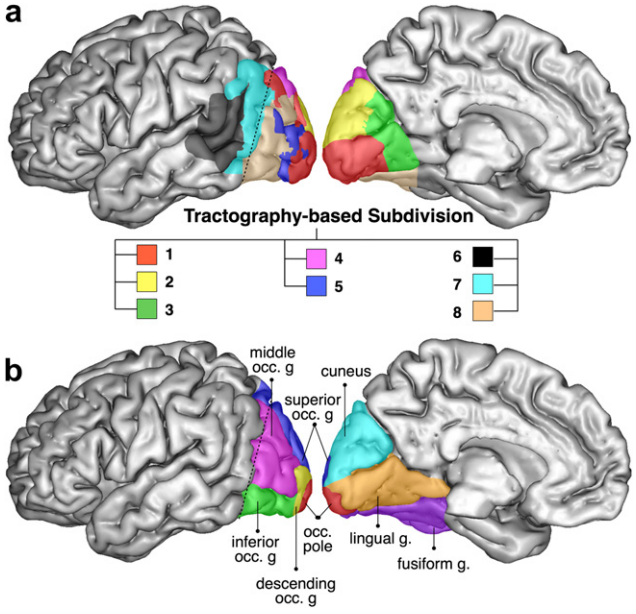

Fig. 2 – Parcellation of the left occipital lobe (a) Lateral and medial views of the group result of the tractography-based parcellation for the left occipital lobe. (b) Classical sulco-gyral anatomy of the left occipital lobe.

2.6. Asymmetries

For each lobe, the volume of the eight clusters registered with the MPRAGE dataset was extracted using FSL and a lateralisation index was calculated according to the following formula:

$$(\text{Volume Right} - \text{Volume Left})/(\text{Volume Right} + \text{Volume Left})$$

Statistical significance of the degree of lateralisation was determined using a one-sample t test for each tract. Only results that survived Bonferroni correction ($p < .00625$) are reported in Fig. 5a.

2.7. Myeloarchitectonic, cytoarchitectonic, myelogenetic, lesion-based and functional maps subdivisions

The maps displayed in Fig. 7a–d are coloured reproductions of the original descriptions reported: (i) in Smith (1907) for the myeloarchitectonic subdivision (Fig. 7a), (ii) in Amunts et al. (2000), Rottschy et al. (2007), Malikovic et al. (2007), Kujovic et al. (2012) and Caspers et al. (2006, 2008, 2012) for the cytoarchitectonic subdivision (Fig. 7b), (iii) in Holmes (1918) for the lesion-based subdivision (Fig. 7c), (iv) in Flechsig (1920) for the myelogenetic subdivision (Fig. 7d) and (v) in Van Essen (2003) for the functional map subdivision (Fig. 7e).

2.8. rsfMRI covarying networks

For the rsfMRI covarying networks, we used an independent component analysis in order to decompose the rsfMRI of our participants into a set of distinct spatial maps, each with its own distinct time course (Kiviniemi et al., 2003; Smith, 2011).

In brief, fMRI data was analysed using the standard set of tools implemented in the FSL software package (Multivariate Exploratory Linear Optimized Decomposition into Independent Components – multivariate exploratory linear optimized decomposition into independent components (MELODIC), http://www.fmrib.ox.ac.uk/fsl/) (Beckmann et al., 2005; Smith et al., 2004). fMRI datasets were corrected for head motion by rigid registration to the first volume (Jenkinson et al., 2002), capped with a high pass filter (.01 Hz, Gaussian-weighted least-squares straight line fitting, with sigma = 50.0 sec) and skull-stripped (Smith, 2002). Each subject's fMRI data was registered to that subject's high-resolution structural image (Jenkinson et al., 2002) and then registered again, this time, with the standard Colin27 template using affine (FLIRT) and non-linear registration (FNIRT). In order to obtain a steady-state signal, the ten first volumes of each dataset were discarded from the analyses. All resulting datasets were concatenated in the temporal dimension. This approach is

Please cite this article in press as: Thiebaut de Schotten M, et al., Subdivision of the occipital lobes: An anatomical and functional MRI connectivity study, Cortex (2012), http://dx.doi.org/10.1016/j.cortex.2012.12.007

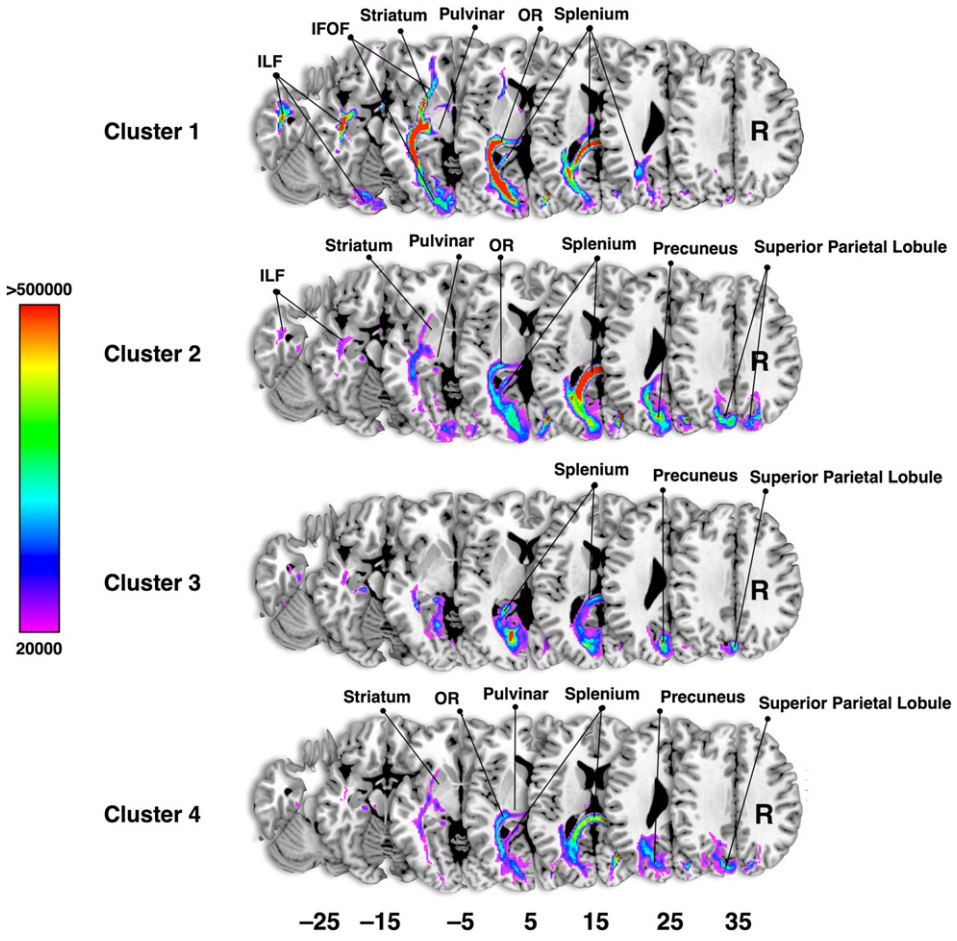

Fig. 3 – Anatomical connectivity for each of the clusters 1–4 identified in the left occipital lobe. The outline of the pattern of anatomical connectivity for each cluster is summarised in table. Precuneus, ipsilateral connections to the precuneus; Splenium, splenium of the corpus callosum; OR, optic radiations; Pulvinar, projections from the pulvinar; Striatum, projections from the striatum.

advantageous, as it does not assume that the associated temporal response is consistent across subject but rather looks for common spatial patterns between subjects. Analysis was carried out using probabilistic independent component analysis (Beckmann and Smith, 2004) as implemented in MELODIC Version 3.10, part of FSL package.

3. Results

3.1. *Tractography-based parcellation*

Overall, probabilistic tractography combined with principal component analysis statistical framework revealed eight clusters sharply segregated, from which seven were in the occipital lobe (freely downloadable at http://www.natbrainlab.com or on demand michel.thiebaut@gmail.com), each showing a specific pattern of connections with the rest of the brain (see Table 1) and for most, being symmetrically distributed among the two hemispheres.

Cluster 1 included the occipital pole and the posterior part of the descending occipital, lingual, fusiform gyri and the posterior lower lip of the calcarine fissure (Fig. 2). Tractography from cluster 1 revealed anatomical connectivity with the rest of the brain conveyed by long-range pathways such as the inferior longitudinal fasciculus (ILF), the inferior fronto-occipital fasciculus (IFOF), the splenium of the corpus callosum, the optic radiations as well as connections to the pulvinar and the striatum (Fig. 3). As illustrated in Fig. 5a, cluster 1 was symmetrically distributed among the two hemispheres ($t = -.676$, $p = .509$).

Cluster 2 extended mainly on the medial surface of the occipital lobe and included the medial portion of the superior occipital gyrus, the posterior part of the cuneus and the posterior upper lip of the calcarine fissure (Fig. 2). This cluster was anatomically connected with the rest of the brain via the splenium of the corpus callosum, the optic radiations, the ILF, and to the pulvinar and the striatum. Tractography also revealed bilateral connections of this cluster with the precuneus and the superior parietal lobule (Fig. 3). Cluster 2 was significantly larger in the right hemisphere when compared to the left ($t = 3.170$, $p = .006$). This difference survived Bonferroni correction for multiple comparisons (Fig. 5a).

Please cite this article in press as: Thiebaut de Schotten M, et al., Subdivision of the occipital lobes: An anatomical and functional MRI connectivity study, Cortex (2012), http://dx.doi.org/10.1016/j.cortex.2012.12.007

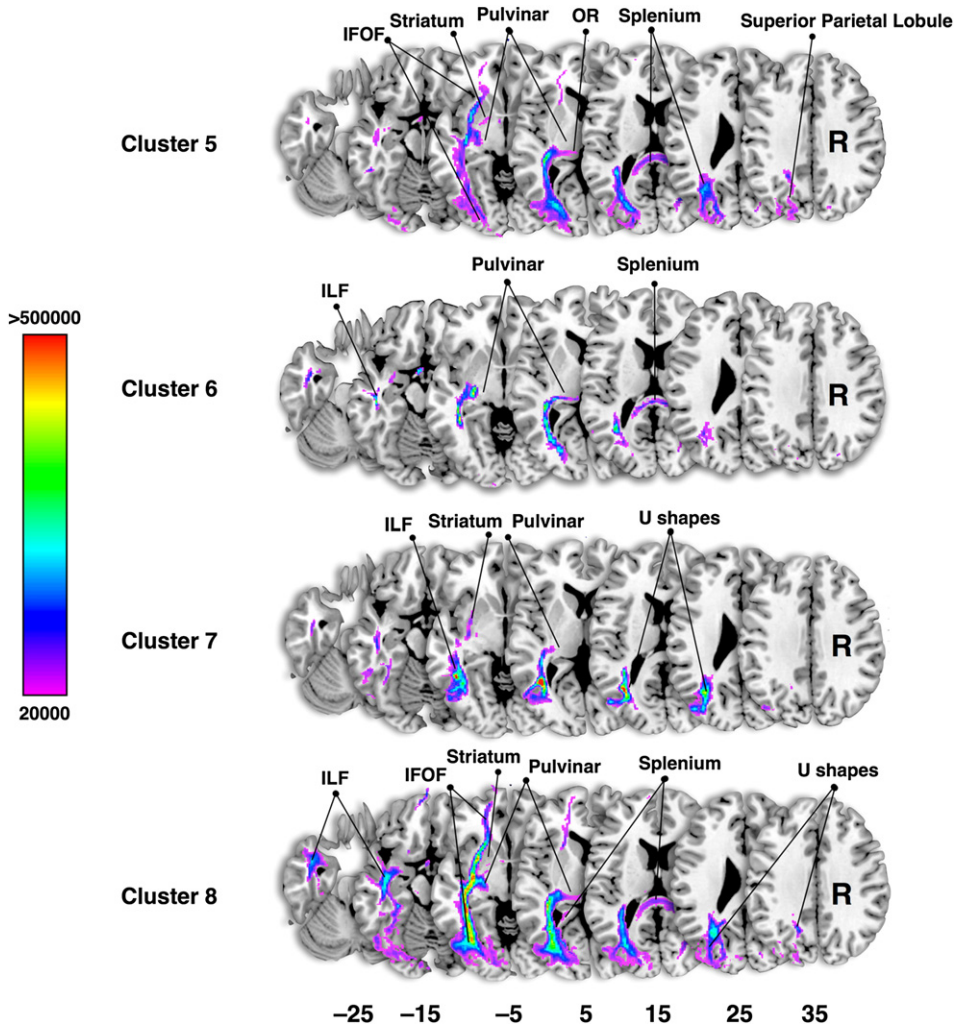

Fig. 4 – Anatomical connectivity for each of the clusters 5–8 identified in the left occipital lobe. The outline of the pattern of anatomical connectivity for each cluster is summarised in Table 1. SPL, ipsilateral connections to the superior parietal lobule; Splenium, splenium of the corpus callosum; Pulvinar, projections from the pulvinar; Striatum, projections from the striatum; U shapes, local connections.

Cluster 3 was situated in the medial surface of the occipital lobe lying behind the occipito-parietal sulcus. It included the anterior portion of the lingual, cuneus gyri and striate cortex (Fig. 2). Cluster 3's anatomical connectivity was mainly conveyed via the splenium of the corpus callosum and short connection to the precuneus and the superior parietal lobule of the left hemisphere (Fig. 3). Cluster 3 was symmetrically distributed among the two hemispheres ($t = .129$, $p = .899$) (Fig. 5a).

Cluster 4 lied on the dorsolateral portion of the occipital lobe, and included the anterior-dorsal part of the superior occipital gyrus (Fig. 2). This cluster was anatomically connected with the rest of the brain via the splenium of the corpus callosum, the optic radiations, to the pulvinar and the striatum, and bilaterally connected to the precuneus and the superior parietal lobule (Fig. 3). There was no significant asymmetry between the left and the right clusters 4 ($t = -.470$, $p = .645$) (Fig. 5a).

Cluster 5 was visible on the lateral surface of the occipital lobe and included the descending occipital gyrus and a small portion of the middle occipital gyrus (Fig. 2). Tractography seeded from this cluster revealed anatomical connections with the rest of the brain via the IFOF, optic radiations, splenium of the corpus callosum, and had connections to the ipsilateral superior parietal lobule, the pulvinar and the striatum (Fig. 4). Cluster 5 showed a rightward trend of hemispheric lateralisation, which was not significant ($t = 1.759$, $p = .10$) (Fig. 5a).

Cluster 6 was located, in most of the participants, outside the occipital lobe and included the posterior portion of the superior and middle temporal gyri and sometimes the most anterior portion of the middle occipital gyrus (Fig. 2). Tractography of the occipital portion of the cluster 6 revealed anatomical connections with the rest of the brain conveyed via the ILF, the splenium of the corpus callosum and connections to the pulvinar (Fig. 4). Cluster 6 was symmetrically distributed among the two hemispheres ($t = .474$, $p = .643$) (Fig. 5a).

Cluster 7 was situated halfway between the occipital, the parietal and the temporal lobes and included the most

Please cite this article in press as: Thiebaut de Schotten M, et al., Subdivision of the occipital lobes: An anatomical and functional MRI connectivity study, Cortex (2012), http://dx.doi.org/10.1016/j.cortex.2012.12.007

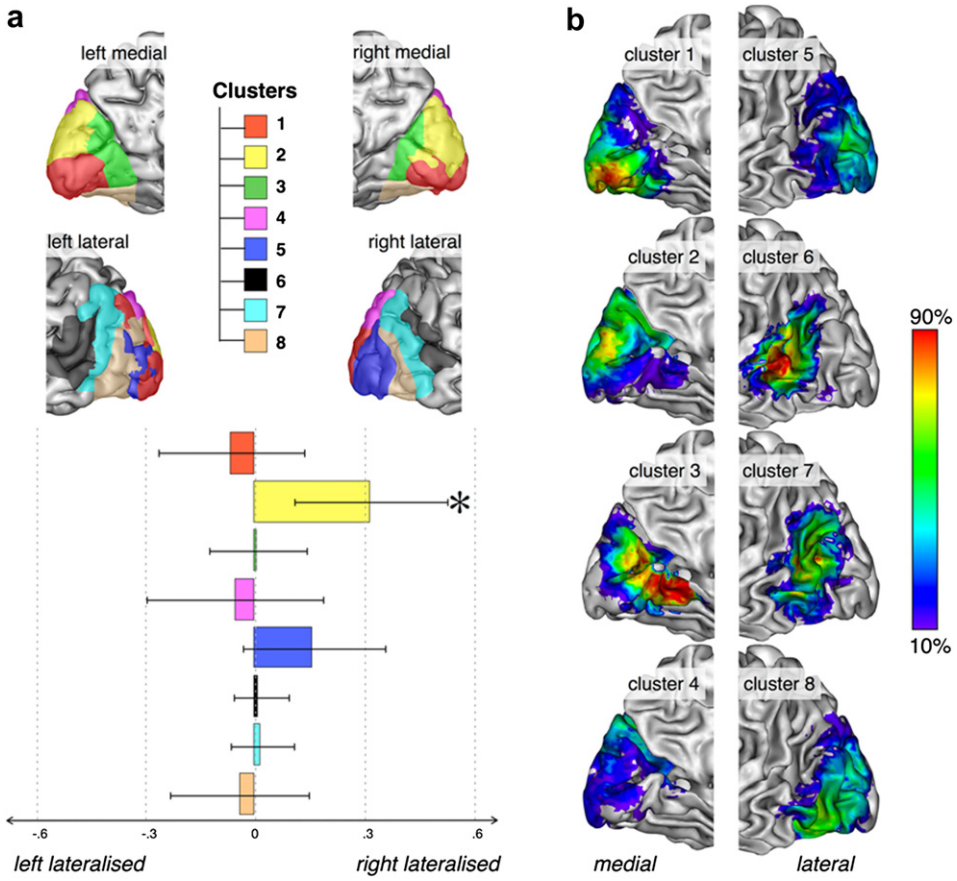

Fig. 5 – Inter-individual variability of the tractography-based parcellation. (a) Lateralisation index for the volume of the eight clusters as revealed by tractography-based parcellation. *$p < .05$ after correction for multiple comparisons. (b) Percentage overlap of the eight reported clusters visualised on medial (left) or lateral (right) view of the occipital cortex.

posterior portion of the middle temporal gyrus, the posterior part of the angular gyrus and the anterior part of the middle occipital gyrus (Fig. 2). Individual tractography of the occipital portion of the cluster 6 revealed connections with the rest of the brain via the ILF, and connections to the pulvinar and the striatum (Fig. 4). No significant asymmetry between the left and the right clusters 7 was found ($t = .482$, $p = .636$) (Fig. 5a).

Cluster 8 included most of the middle occipital and inferior occipital gyri (Fig. 2). Its anatomical connectivity was mainly conveyed via the ILF, the IFOF, the optic radiations, the splenium of the corpus callosum and connections to the pulvinar, the striatum and the ipsilateral superior parietal lobule (Fig. 4). Cluster 8 was symmetrically distributed among the two hemispheres ($t = -.462$, $p = .651$) (Fig. 5a).

The probability maps obtained for the group revealed that the tractography-based parcellation has a concentric distribution with a descending gradient from the central portion (overlap of more than 90%) to the most peripheral zones (overlap above 50%) (Fig. 5b).

3.2. *rsfMRI covarying networks*

Overall, resting state connectivity combined with independent component analysis statistical framework revealed 32 resting brain networks, each having its own distinct time course. Five of these networks included parts of the occipital lobe (Figs. 6 and 7f).

Covarying network 1 included activations in the occipital pole and, the inferior, middle and superior occipital gyri, the posterior part of the fusiform gyrus and superior parietal lobule. In addition, de-activation in the posterior part of the cingulate cortex was also observed. This network matched the description of the lateral visual cortical network identified with rsfMRI by Beckmann et al. (2005) and Smith et al. (2009). The peak of frequency was ~.02 Hz for this network.

Covarying network 2 was observed on the medial surface and included the cuneus and the lingual gyri and matched the original description of the medial visual cortical network originally reported by Beckmann et al. (2005) and Smith et al. (2009) using rsfMRI. This network showed maximum resting oscillation between ~.06 and ~.07 Hz.

Covarying network 3 was situated mostly in the medial surface including activations in the most anterior portion of the cuneus, the posterior portion of the precuneus, the superior parietal lobule, the posterior and anterior cingulate gyri and was similar to the default network (Greicius et al., 2003; Raichle et al., 2001; Raichle and Snyder, 2007). This network had a peak of frequency at ~.02 Hz.

Please cite this article in press as: Thiebaut de Schotten M, et al., Subdivision of the occipital lobes: An anatomical and functional MRI connectivity study, Cortex (2012), http://dx.doi.org/10.1016/j.cortex.2012.12.007

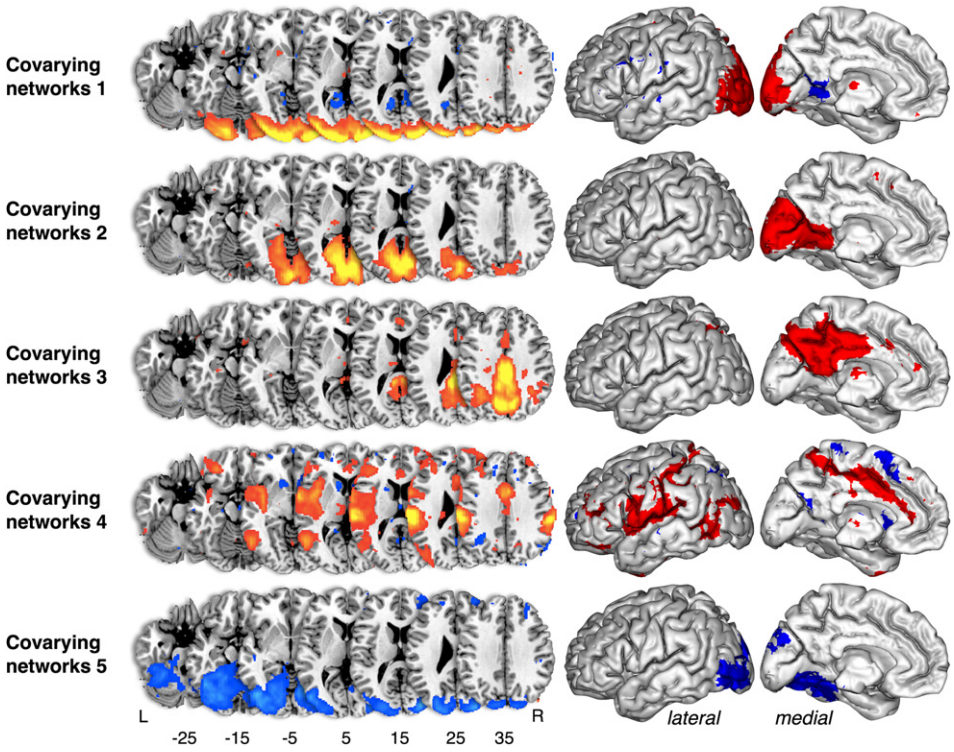

Fig. 6 – Covarying networks involving the occipital lobe. On the left panel red to yellow gradient represents areas covarying positively whereas dark to light blue gradient corresponds to areas covarying negatively. On the right panel red colour indicates areas covarying positively whereas blue colour corresponds to areas covarying negatively.

Covarying network 4 was situated halfway between the occipital, temporal and the parietal lobes and included the posterior part of the angular gyrus and the anterior part of the middle and inferior occipital gyri. More anteriorly, this network included the insula, the lateral orbital and middle frontal gyri. Additionally, we noticed de-activations in the superior frontal gyrus, the caudate and the superior parietal lobule. The maximum resting oscillation was centred on ~.09 Hz for this network.

Covarying network 5 was mostly localised on the ventral surface of the occipital lobe including de-activation in part of the fusiform, the inferior occipital and the right middle frontal gyri. This network had a peak of frequency at ~.02 Hz.

4. Discussion

In this study we used DTI probabilistic tractography combined with a principal component analysis to divide the human left and right occipital lobes into several areas, which share similar anatomical connectivity. Three main findings emerge from our work. Firstly, our parcellation successfully identified seven clusters in the occipital lobes, which showed a different pattern of macroscopic anatomical connectivity. Secondly, most of these areas are symmetrically organised except for cluster 2, which is larger in the right hemisphere when compared to the left. Lastly, using rsfMRI-based parcellation in the same group of subjects, we showed that the clusters identified in the occipital lobe with the tractography-based parcellation overlap poorly with the covarying networks in the resting brain.

Tractography-based parcellation methods group together voxels, which share similar patterns of connection with the rest of the brain. This approach segregates anatomical areas in the living human brain that have solely been identified using post-mortem techniques. Similarly to previous studies (Anwander et al., 2007; Johansen-Berg et al., 2004; Mars et al., 2011), our subdivision of the occipital lobe shows some similarities with the lateral surface of previous post-mortem subdivisions in humans, functional subdivisions obtained from monkey electrophysiology, functional imaging in healthy participants and clinical syndromes associated with localised brain damage (Fig. 7).

Cluster 4, for instance, matches the description of the myelogenetic area 15, the visual area V3A and the cytoarchitectonic area hOC4d (Kujovic et al., 2012). fMRI studies revealed that this area is retinotopic (Gardner et al., 2008; Tootell et al., 1998), involved in the processing of 'real' motion, and works independently of retinal motion. This suggests that cluster 4 may play a role in perceptual stability during eye movements (Braddick et al., 2001; Fischer et al., 2012; Tootell et al., 1997). Surprisingly, in the rare cases reporting a stroke lesion in this region (Kraft et al., this issue) this area is not associated with visual motion blindness (i.e., akinetopsia), but is rather linked with impaired spatial awareness of more than one object at a time (simultagnosia, see Chechlacz et al., 2012).

Akinetopsia is more likely to follow a bilateral lesion in the area MT+, which lies on the posterior bank of the

Please cite this article in press as: Thiebaut de Schotten M, et al., Subdivision of the occipital lobes: An anatomical and functional MRI connectivity study, Cortex (2012), http://dx.doi.org/10.1016/j.cortex.2012.12.007

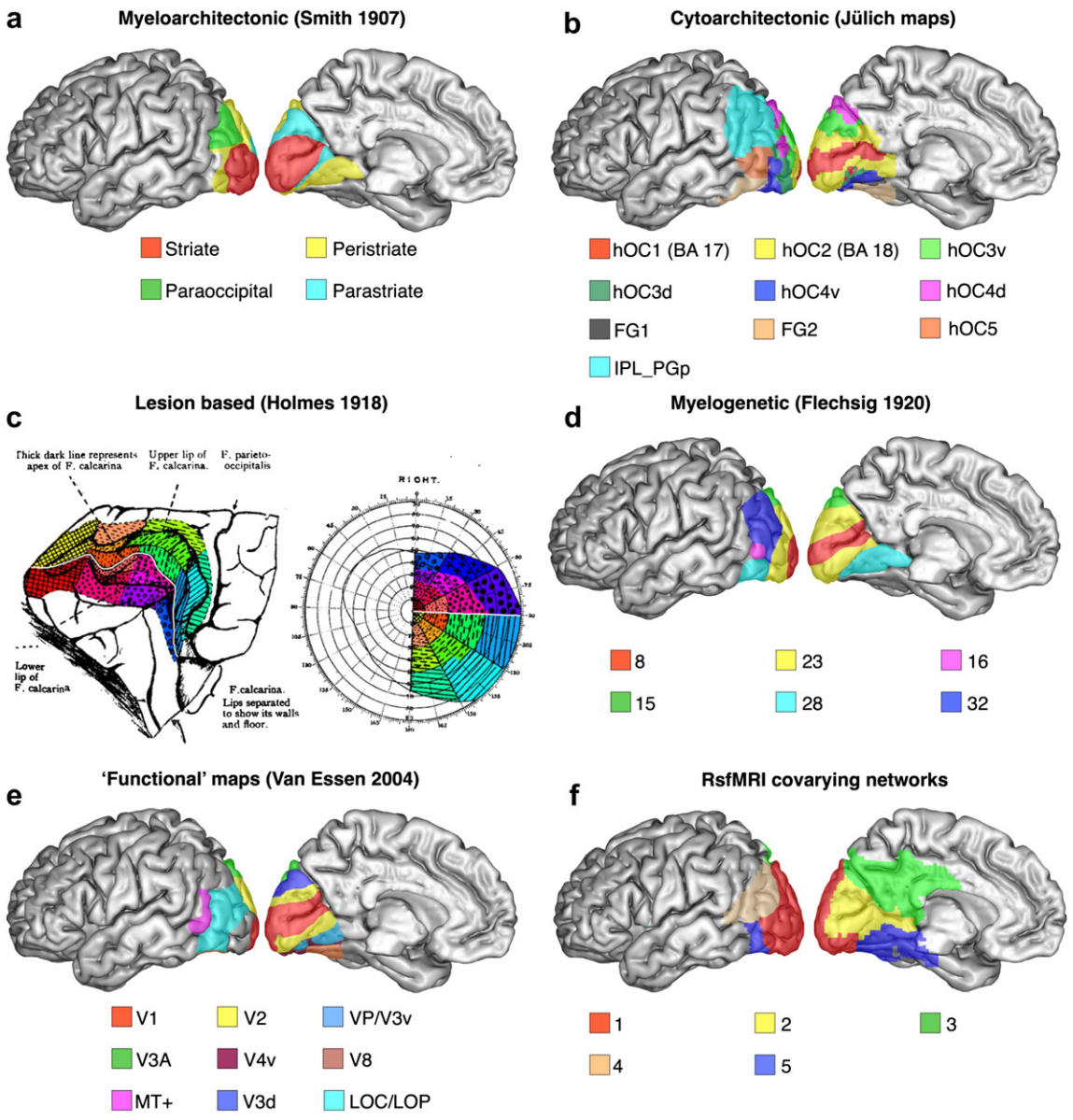

Fig. 7 – Subdivisions of the occipital lobe based on (a) the density of myelinated fibres (i.e., myeloarchitectonic) (Smith, 1907) (b) the visible variation in the neuronal pattern of the six cortical layers (i.e., cytoarchitectonic) (Brodmann, 1909), (c) the visual impairment after brain lesion (Holmes, 1918), (d) the progressive myelination during maturation of the human forebrain (Flechsig, 1920), (e) the monkey to human geometric translation of the subdivision of visually responsive cortex based on direct electrical recording (Van Essen, 2003) and (f) covarying networks involving the occipital lobe. Please note that there is no colour correspondence between the six subdivisions.

superior temporal sulcus, corresponding to the inferior part of cluster 7 (Kraft et al., this issue; Rizzo et al., 1995; Zeki, 1991) and area hOC5 (Malikovic et al., 2007). fMRI studies report this area as being spatiotopic anteriorly (d'Avossa et al., 2007) and retinotopic posteriorly (Gardner et al., 2008). fMRI studies also reveal that this area is involved in the processing of motion stimuli (Bartels et al., 2008), this time, responding equally to retinal motion and 'real' motion (Fischer et al., 2012). Whether akinetopsia intervenes after a very localised lesion in the highly specific area MT+ (inferior part of cluster 7) or after a disruption of the tract between MT+ and V3A (cluster 4) (Vergani et al., this issue) remains to be clarified in future lesion-symptoms studies.

Cluster 8 overlapped with lateral occipital central/lateral occipital peripheral (LOC/LOP) (V7) and V8 (Fig. 2a), FG2 and HOC5 (Fig. 2b; Caspers et al., 2012), and the rsfMRI covarying network 5. These areas do not precisely correspond to any myeloarchitectural, or myelogenitical subdivisions known. LOC/LOP and V8 are both involved in the extraction of object features. LOC/LOP extracts general information about an object's structure (Kourtzi and Kanwisher, 2000) and has been shown to participate in visual recognition (Grill-Spector et al., 2000; Ungerleider and Mishkin, 1982) and body-part

Please cite this article in press as: Thiebaut de Schotten M, et al., Subdivision of the occipital lobes: An anatomical and functional MRI connectivity study, Cortex (2012), http://dx.doi.org/10.1016/j.cortex.2012.12.007

Table 1 – Connections identified seeding tractography from the occipital portion of the eight tractography-based parcellated clusters. SPL, ipsilateral connections to the superior parietal lobule; Precuneus, ipsilateral connections to the precuneus; Splenium, splenium of the corpus callosum; Pulvinar, projections from the pulvinar; Striatum, projections from the striatum.

		Clusters							
		1	2	3	4	5	6	7	8
Association pathways	ILF (temporal)	+	+	–	–	–	+	+	+
	IFOF (frontal)	+	–	–	–	+	–	–	+
	SPL	–	+	+	+	+	–	–	+
	Precuneus	–	+	+	+	–	–	–	–
Commissural pathway	Splenium (opposite hemisphere)	+	+	+	+	+	+	–	+
Projection pathways	OR (lateral geniculate nucleus)	+	+	–	+	+	–	–	+
	Pulvinar	+	+	–	+	+	+	+	+
	Striatum	+	+	–	+	+	–	+	+

perception (Astafiev et al., 2004). In functional imaging, the lower portion of LOC/LOP is functionally activated during the visual recognition of objects (Cavina-Pratesi et al., 2010a, 2010b; James et al., 2000; Sergent et al., 1992). When damaged by a stroke, this area is associated with an incapacity to recognise objects either due to an alteration of early-level perceptual processing (i.e., apperceptive agnosia) (Ferreira et al., 1998; Warrington and James, 1988) or the inability to group component parts of an object into a coherent whole (i.e., integrative agnosia) (Behrman and Kimchi, 2003; Riddoch and Humphreys, 1987; Riddoch et al., 2008). Alternatively, V8, which is localised in the fusiform gyrus, is more specialised in the recognition of faces (Sergent et al., 1992), colours (Hadjikhani et al., 1998) and words (Cohen et al., 2000), as revealed by fMRI and positron emission tomography (PET) studies in healthy participants. When damaged, this same area is also associated with the incapacity to recognise faces (prosopagnosia) (Kleinschmidt and Cohen, 2006; Kraft et al., this issue), colours (achromatopsia) (Bartolomeo et al., this issue; Kraft et al., this issue; Verrey, 1888) and words (pure alexia) (Dejerine, 1895; Epelbaum et al., 2008; Gaillard et al., 2006). Overall, our cluster 8 appears to overlap with areas (LOC/LOP and V8) where early recognition of visual stimuli occurs.

Cluster 5 matches the functionally unidentified area situated between LOC/LOP and V2 (Van Essen, 2003), in cytoarchitectonic subdivision hOC4v (Rottschy et al., 2007) and the myelogenetic area 23 (Flechsig, 1920). To our knowledge, precise anatomo-functional correlates of this cluster are still poorly known and remain to be explored using fMRI in humans and electrical recording in animals.

The medial view of our tractography-based parcellation shows clear differences with classical myeloarchitectural (Smith, 1907), cytoarchitectural (Amunts et al., 2000; Brodmann, 1909; Caspers et al., 2012, 2008, 2006; Kujovic et al., 2012; Malikovic et al., 2007; Rottschy et al., 2007), myelogenetical (Flechsig, 1920), functional maps (Van Essen, 2003), and the covarying networks in the resting brain. Although these differences may be due to the limitations of the method (discussed further in this paper), in this section we will discuss their potential for functional interpretation.

The cortical areas processing the lower and upper visual fields are retinotopic (Gardner et al., 2008; Tootell et al., 1998) and have a similar organisation in terms of myeloarchitecture (striate, parastriate, peristriate) (Fig. 7a), cytoarchitecture (BA17, BA18, BA19) (Fig. 7b), progressive myelination during maturation (areas 8 and 23) (Fig. 7d) and functional (V1, V2, V3) organisation (Fig. 7e). However, we report a subdivision between two clusters, one below (cluster 1) and one above (cluster 2) the calcarine sulcus, each receiving input from the upper and the lower visual fields respectively (Fig. 7c). Brain regions representing the lower and upper fields in the visual cortex differ in regards to their neuronal input and output. Concerning inputs, the distribution of ganglion cells across the retina is not uniform, the density of ganglion cells is approximately 60% greater in the superior retina (i.e., lower visual field) than in the lower retina (Curcio et al., 1987). This asymmetry persists along the visual stream up to ventral and dorsal primary visual areas, where visual outputs to the rest of the brain are also segregated into ventral and dorsal visual pathways, respectively (Van Essen et al., 1986). Similar projections have been hypothesized in humans (Previc, 1990) and are supported by clinical observations. When damaged, cluster 1 (under calcarine) is associated with upper quadrantic field defects and cluster 2 (above calcarine) is associated with inferior quadrantic field defects (for a review see ffytche et al., 2010; Holmes, 1918; Horton and Hoyt, 1991). Our tractography-based parcellation shows, for the first time, a clear dissociation in the connectivity pattern between the occipital regions representing the lower and the upper visual fields, regardless of cytoarchitecture and myeloarchitecture. Hence, our parcellation suggests a distinction in the anatomical connectivity between the cortex dedicated to the superior visual field and the cortex dedicated to the inferior visual field. One may putatively stipulate that the inferior visual field, located in the dorsomedial occipital cortex, would be more inclined to connect with the visual dorsal stream 'how/where' (Kravitz et al., 2011; Ungerleider and Mishkin, 1982), whereas the superior visual field, located in the ventromedial occipital cortex, would most likely be better connected with the visual ventral stream 'what'(Kravitz et al., 2011; Ungerleider and Mishkin, 1982). Our anatomical data supports this hypothesis, as cluster 1, in the ventromedial occipital cortex which processes information from upper visual field, is highly connected to the temporal cortex via the ILF, and to the orbitofrontal cortex via the IFOF; while the cluster 2, in the dorsomedial occipital cortex, which processes information from lower visual field, is highly connected to the precuneus and the superior parietal lobule (see Table 1). The observed differences in the connectivity pattern may be an explanation to the behavioural differences in the processing of visual information in the upper and lower visual fields. Several studies have reported dominance of the lower visual field for coordinate judgement, and in the upper visual field for categorical judgement (Niebauer and Christman, 1998). The lower visual field has also been reported as dominant, when compared to the upper visual field for the processing of visual information in peripersonal space, and for the processing small movement contrast or hue, whereas the upper visual field has been

Please cite this article in press as: Thiebaut de Schotten M, et al., Subdivision of the occipital lobes: An anatomical and functional MRI connectivity study, Cortex (2012), http://dx.doi.org/10.1016/j.cortex.2012.12.007

associated with a better processing of information in extrapersonal space (Levine and McAnany, 2005; Previc, 1990).

Our parcellation also shows a further subdivision of the primary visual areas with cluster 3, localised in the retinotopic representation of the peripheral visual field, without any further segregation between lower and upper field. In addition, cluster 3 also showed weak anatomical connectivity with the rest of the brain, including the absence of connection with the lateral geniculate nuclei via the optic radiations. Whether this third cluster is a real or artificial subdivision, remains to be clarified (see limitations paragraph). Alternatively, this cluster may correspond to the visual brain area in charge of the peripheral visual field processing (Fig. 7c). As for the upper and the lower visual fields, brain regions representing central and peripheral fields in the visual cortex differ in regards to their neuronal input and output. In the retina, distribution of ganglion cells varies with eccentricity; the midget ganglion cells are mainly present in the central retina, while parasol ganglion cells represent 90% of the ganglion cells in the peripheral retina (Dacey, 1993; Dacey and Petersen, 1992). Midget and parasol cells project, respectively, to the parvocellular and the magnocellular layers of the lateral geniculate body (Leventhal et al., 1985). Central vision receives its inputs largely from the parvocellular visual pathways and peripheral vision the magnocellular pathways (Meissirel et al., 1997). Consequently, the antero-occipital region (cluster 3), involved in peripheral vision, receives inputs mainly from magnocellular pathways, while the posterior region (clusters 1 and 2) receives inputs principally from parvocellular visual pathways. The distinction between central and peripheral vision is also maintained all along the visual information processing streams. Indeed, dorsal stream areas receive relatively more projections from areas processing peripheral visual field representations, whereas ventral stream areas are more densely connected to those processing central representations (Gattass et al., 2005; Ungerleider and Desimone, 1986). The peripheral/central vision segregation can be observed up to the frontal cortex. Fibres from the ventral visual pathways are projected preferentially to the orbito-frontal cortex, while those from the dorsal pathways are projected towards the dorsolateral prefrontal cortex (Wilson, 1993). The central vision is also more sensitive to colour vision, and high spatial frequencies. It would mainly be involved in object recognition, while peripheral vision is more sensitive to low spatial frequencies or moving stimuli, and would be essential for detecting sudden changes in the environment. Other authors also reported dissociation in favour of peripheral vision for the processing of facial expressions (Bayle et al., 2009, 2011). Lesion studies support the association between peripheral vision and the dorsal stream. Lesion to the parieto-occipital cortex containing dorsal stream areas results in optic ataxia, which manifests in the peripheral vision (Pisella et al., 2006) and impairs perception in the periphery (Pisella et al., 2009). In other words, there is a partial structural separation between central and peripheral vision processing pathways, from the retina, to V1, as well as to higher-level visual areas. The differences in the nature of the input and the output of the central primary visual cortices when compared to the peripheral primary visual cortices may support the difference in connectivity patterns between clusters 1 and 2 and more anteriorly with cluster 3. This anatomical segregation is also coherent with the functional properties of peripheric and central vision.

Cluster 2 was significantly reported as larger in the right hemisphere. This result is consistent with previous work reporting the right hemisphere as dominant for visuospatial processing (Heilman and Van Den Abell, 1980; Thiebaut de Schotten et al., 2011a), and the lower-field advantage for spatio-attentional tasks (Bayle et al., 2011; Danckert and Goodale, 2001; Kraft et al., 2007). The functional dissociation between the upper and lower visual fields reported in the previous paragraph suggests that the hemispheric asymmetry of cluster 2 should also be associated with a better judgement for spatio-attentional tasks in the lower left quadrant as compared to the lower right quadrant. Line bisection test is a spatio-attentional task that requires estimating the centre of a 20-cm line usually presented in the lower visual field of the participant. In the general population, a small left deviation in the line bisection test is observed and referred to as the 'pseudoneglect effect' (Jewell and McCourt, 2000). This left deviation in the line bisection is usually regarded as a manifestation of an asymmetrical processing of visuospatial information in the normal brain. Hence, cluster 2 and its connections with the rest of the brain may induce the 'pseudoneglect effect'.

No clear equivalence was found between the tractography-based parcellation and the rsfMRI covarying networks. Whilst rsfMRI covarying networks did not seem either to respect any of the standard myelogenetic, myelo and cytoarchitectonic boundaries, pioneers studies demonstrate that some rsfMRI covarying networks closely match brain's functional architecture during activation (Fox et al., 2006; Smith et al., 2009). Nevertheless, it is important to insist on the fact that rsfMRI covarying networks reflect correlation in the metabolism between distant brain areas. This correlation does not correspond to a direct measure of correlated neuronal activity, but rather co-variations in the blood-oxygen level dependant signal (Fox and Raichle, 2007). Further work would be required to determine whether all metabolic correlations reported with rsfMRI measures correspond to brain's functional architecture during activation and are an indirect measure of neuronal synchronisation, or if they solely reflect a residual variability in blood flow.

Another limitation in our study concerns the use of probabilistic tractography between the seeds and targets as a surrogate for the 'anatomical connectivity' strength. *Stricto sensu* probabilistic tractography does not provide an index of anatomical connectivity from one area to another in the brain, it offers an estimate of the mathematical confidence we can have in the reconstruction of a given pathway for a given dataset (Jones, 2010). Although many previous studies have used it, the estimation it provides may also not systematically hold true due to an inherent DTI tractography limitation, as tractography may miss fibre crossing and fanning (=false negative) or reconstruct spurious connections in the case of kissing and intertwining configurations (=false positive). This limitation may account for the existence of cluster 3, which according to our tractography, is missing projections from the lateral geniculate nuclei via the optic radiations. Likewise, connections through the splenium of the callosum are

Please cite this article in press as: Thiebaut de Schotten M, et al., Subdivision of the occipital lobes: An anatomical and functional MRI connectivity study, Cortex (2012), http://dx.doi.org/10.1016/j.cortex.2012.12.007

identified in all the clusters with the exception of cluster 7. However, the results from tracer studies on non-human primates suggest that the callosal connections are restricted to the vertical Meridian of primary visual cortex and are very sparse in the horizontal Meridian and in general in area 17 (Cusick et al., 1984; Van Essen et al., 1982). This discrepancy is likely due to the merging of the callosal fibres with the optic radiations, in other words, an artefact of the tractography technique. This may also explain why we did not find a distinction between V1 and V2 with our tractography-based parcellation.

V1 and V2 show more differences in their pattern of short U shape connections than in the way they are connected to the rest of the brain via long-range white matter pathways (Felleman and Van Essen, 1991; Zilles and Clarke, 1997). Our tractography may have missed these short connections leading the principal component analysis to group these two areas together. It is interesting to note that rsfMRI did not differentiate these areas either.

The resolution of diffusion imaging certainly modifies the level of detail in reported anatomical connectivity. We suspect the number of identified clusters as being intimately limited by this level of detail. Future studies employing high-resolution fibre crossing algorithms combined with high spatial resolution datasets (Dell'acqua and Catani, 2012; Dell'Acqua et al., 2009; Dell'Acqua et al., 2007; Dell'Acqua et al., 2012) are required to confirm and further detail the tractography-based subdivision of the occipital lobe.

We employed different statistical framework for the tractography-based parcellation and the identification of rsfMRI covarying networks, which may explain some of the differences found between these two subdivisions of the occipital lobe. In the case of the tractography-based parcellation, we chose a principal component analysis rather than independent component analysis as we had no assumption for the non-gaussianity of the distribution of the principal components (Bugli and Lambert, 2006). For the resting state functional connectivity-based parcellation, we employed a standard probabilistic independent component analysis, which has previously been optimised by other groups for the analysis of the rsfMRI (Beckmann et al., 2005; Beckmann and Smith, 2004). Both principal and independent component analyses are linear transformation methods for multivariate data, and identify components that are linear combinations of all the original variables. Recent new methods also consider non-linear combination for dimension reduction, such as sparse principal component analysis (Zou et al., 2006). Future research of tractography-based parcellation based on sparse principal component analysis may test whether non-linear is more appropriate than a linear combination in the case of tractography-based parcellation of the human brain.

Current tensor models are unable to extract reliable directional information in the grey matter. Our method tries to circumvent this problem by creating a white matter ribbon directly beneath the grey matter ribbon, and uses it as seed regions. This white matter ribbon may contain axonal connections from spatially distant cortical regions, and therefore grey matter voxel directly above may not match the subjacent white matter ribbon. This may account for the variations observed between the tractography-based parcellation and the independent component analysis of rsfMRI data. The same effect may also explain discrepancy between the tractography-based parcellations and other cortical parcellations.

Gender differences were not estimated in our study due to the small size of the sample (10 males and eight females). Future studies will need to compare gender differences in a larger dataset.

In conclusion, our study reports seven brain areas in each occipital lobe showing different patterns of anatomical connectivity. Although this subdivision of the occipital lobe is unique, in the sense that it does not correspond exactly to standard myeloarchitectonic, cytoarchitectonic and myelogenetic subdivisions, it showed consistency with functional properties of occipital areas, identified by functional imaging studies in healthy controls or cognitive profiles in brain-damaged patients. Such parcellation, based on the connectional anatomy, offers a new promising subdivision of the living human brain, which may assist in the understanding of clinical-neuroanatomical dissociations and functional neuroimaging results.

Acknowledgements

This work was supported by the French *Agence Nationale de la Recherche* (project CAFO-RPFC, No: ANR-09-RPDOC-004-01 and project HM-TC, No: ANR-09-EMER-006). We would like to thank the members of Forschungszentrum Jülich GmbH for providing us with the cytoarchitectonic maps of the occipital lobe, the Natbrainlab for discussions and for their help during various stages of our project, Dominic ffytche, Jean Daunizeau, Marco Catani, Paolo Bartolomeo, Angela Sirigu and Lauren Sakuma.

REFERENCES

Amunts K, Malikovic A, Mohlberg H, Schormann T, and Zilles K. Brodmann's areas 17 and 18 brought into stereotaxic space – Where and how variable? *NeuroImage*, 11(1): 66–84, 2000.

Anwander A, Tittgemeyer M, von Cramon DY, Friederici AD, and Knosche TR. Connectivity-based parcellation of Broca's area. *Cerebral Cortex*, 17(4): 816–825, 2007.

Astafiev SV, Stanley CM, Shulman GL, and Corbetta M. Extrastriate body area in human occipital cortex responds to the performance of motor actions. *Nature Neuroscience*, 7(5): 542–548, 2004.

Avants BB, Epstein CL, Grossman M, and Gee JC. Symmetric diffeomorphic image registration with cross-correlation: Evaluating automated labeling of elderly and neurodegenerative brain. *Medical Image Analysis*, 12(1): 26–41, 2008.

Bartels A, Logothetis NK, and Moutoussis K. fMRI and its interpretations: An illustration on directional selectivity in area V5/MT. *Trends in Neurosciences*, 31(9): 444–453, 2008.

Bartolomeo P, Bachoud-Levi AC, and Thiebaut de Schotten M. The connectional anatomy of cerebral achromatopsia: A hodotopic reappraisal of a case report. *Cortex*, this issue.

Basser PJ, Mattiello J, and Le Bihan D. MR diffusion tensor spectroscopy and imaging. *Biophysical Journal*, 66(1): 259–267, 1994.

Basser PJ, Pajevic S, Pierpaoli C, Duda J, and Aldroubi A. In vivo fiber tractography using DT-MRI data. *Magnetic Resonance in Medicine*, 44(4): 625–632, 2000.

Basser PJ and Pierpaoli C. Microstructural and physiological features of tissues elucidated by quantitative-diffusion-tensor MRI. *Journal of Magnetic Resonance B*, 111(3): 209–219, 1996.

Bayle DJ, Henaff MA, and Krolak-Salmon P. Unconsciously perceived fear in peripheral vision alerts the limbic system: A MEG study. *Public Library of Science One*, 4(12): e8207, 2009.

Bayle DJ, Schoendorff B, Henaff MA, and Krolak-Salmon P. Emotional facial expression detection in the peripheral visual field. *Public Library of Science One*, 6(6): e21584, 2011.

Beckmann CF, DeLuca M, Devlin JT, and Smith SM. Investigations into resting-state connectivity using independent component analysis. *Philosophical Transactions of the Royal Society of London. Series B, Biological Sciences*, 360(1457): 1001–1013, 2005.

Beckmann CF and Smith SM. Probabilistic independent component analysis for functional magnetic resonance imaging. *Institute of Electrical and Electronics Engineers Transactions on Medical Imaging*, 23(2): 137–152, 2004.

Behrens TE, Berg HJ, Jbabdi S, Rushworth MF, and Woolrich MW. Probabilistic diffusion tractography with multiple fibre orientations: What can we gain? *NeuroImage*, 34(1): 144–155, 2007.

Behrens TE, Johansen-Berg H, Woolrich MW, Smith SM, Wheeler-Kingshott CA, Boulby PA, et al. Non-invasive mapping of connections between human thalamus and cortex using diffusion imaging. *Nature Neuroscience*, 6(7): 750–757, 2003.

Behrman M and Kimchi R. What does visual agnosia tell us about perceptual organization and its relationship to object perception? *Journal of Experimental Psychology: Human Perception and Performance*, 42(29): 19–42, 2003.

Braddick OJ, O'Brien JM, Wattam-Bell J, Atkinson J, Hartley T, and Turner R. Brain areas sensitive to coherent visual motion. *Perception*, 30(1): 61–72, 2001.

Brodmann K. *Vergleichende Lokalisationslehre der Großhirnrinde: in ihren Prinzipien…ý*. Leipzig, Germany: Barth, 1909.

Bugli C and Lambert P. Comparison between principal component analysis and independent component analysis in electroencephalograms modelling. *Biometrical Journal*, 48(5): 1–16, 2006.

Burkhalter A and Bernardo KL. Organization of corticocortical connections in human visual cortex. *Proceedings of the National Academy of Sciences of the United States of America*, 86(3): 1071–1075, 1989.

Campbell AW. *Histological Studies on the Localisation of Cerebral Function*. Cambridge: Cambridge University Press, 1905.

Caspers J, Zilles K, Eickhoff SB, Schleicher A, Mohlberg H, and Amunts K. Cytoarchitectonical analysis and probabilistic mapping of two extrastriate areas of the human posterior fusiform gyrus. *Brain Structure and Function*, 2012, http://dx.doi.org/10.1007/s00429-012-0411-8.

Caspers S, Eickhoff SB, Geyer S, Scheperjans F, Mohlberg H, Zilles K, et al. The human inferior parietal lobule in stereotaxic space. *Brain Structure and Function*, 212(6): 481–495, 2008.

Caspers S, Geyer S, Schleicher A, Mohlberg H, Amunts K, and Zilles K. The human inferior parietal cortex: Cytoarchitectonic parcellation and interindividual variability. *NeuroImage*, 33(2): 430–448, 2006.

Catani M, Dell'acqua F, Vergani F, Malik F, Hodge H, Roy P, et al. Short frontal lobe connections of the human brain. *Cortex*, 48(2): 273–291, 2012.

Catani M, Jones DK, Donato R, and Ffytche DH. Occipito-temporal connections in the human brain. *Brain*, 126(Pt 9): 2093–2107, 2003.

Catani M, Jones DK, and ffytche DH. Perisylvian language networks of the human brain. *Annals of Neurology*, 57(1): 8–16, 2005.

Catani M and Thiebaut de Schotten M. A diffusion tensor imaging tractography atlas for virtual in vivo dissections. *Cortex*, 44(8): 1105–1132, 2008.

Catani M and Thiebaut de Schotten M. *Atlas of Human Brain Connections*. Oxford: Oxford University Press, 2012.

Cattell RB. The scree test for the number of factors. *Multivariate Behavioral Research*, 1(2): 245–276, 1966.

Cavina-Pratesi C, Kentridge RW, Heywood CA, and Milner AD. Separate channels for processing form, texture, and color: Evidence from FMRI adaptation and visual object agnosia. *Cerebral Cortex*, 20(10): 2319–2332, 2010a.

Cavina-Pratesi C, Kentridge RW, Heywood CA, and Milner AD. Separate processing of texture and form in the ventral stream: Evidence from FMRI and visual agnosia. *Cerebral Cortex*, 20(2): 433–446, 2010b.

Chechlacz M, Rotshtein P, Hansen PC, Riddoch JM, Deb S, and Humphreys GW. The neural underpinnings of simultanagnosia: Disconnecting the visuospatial attention network. *Journal of Cognitive Neuroscience*, 24(3): 718–735, 2012.

Clarke S. Callosal connections and functional subdivision of the human occipital cortex. In Gulyas B, Ottoson D, and Roland P (Eds), *Functional Organization of the Human Visual Cortex*. Oxford: Pergamon Press, 1993: 137–150.

Clarke S and Miklossy J. Occipital cortex in man: Organization of callosal connections, related myelo- and cytoarchitecture, and putative boundaries of functional visual areas. *Journal of Comparative Neurology*, 298(2): 188–214, 1990.

Cohen L, Dehaene S, Naccache L, Lehéricy S, Dehaene-Lambertz G, Hénaff MA, et al. The visual word form area: Spatial and temporal characterization of an initial stage of reading in normal subjects and posterior split-brain patients. *Brain*, 123(Pt 2): 291–307, 2000.

Conturo TE, McKinstry RC, Aronovitz JA, and Neil JJ. Diffusion MRI: Precision, accuracy and flow effects. *NMR Biomedicine*, 8(7–8): 307–332, 1995.

Curcio CA, Sloan Jr KR, Packer O, Hendrickson AE, and Kalina RE. Distribution of cones in human and monkey retina: Individual variability and radial asymmetry. *Science*, 236(4801): 579–582, 1987.

Cusick CG, Gould 3rd HJ, and Kaas JH. Interhemispheric connections of visual cortex of owl monkeys (*Aotus trivirgatus*), marmosets (*Callithrix jacchus*), and galagos (*Galago crassicaudatus*). *Journal of Comparative Neurology*, 230(3): 311–336, 1984.

d'Avossa G, Tosetti M, Crespi S, Biagi L, Burr DC, and Morrone MC. Spatiotopic selectivity of BOLD responses to visual motion in human area MT. *Nature Neuroscience*, 10(2): 249–255, 2007.

Dacey DM. The mosaic of midget ganglion cells in the human retina. *Journal of Neuroscience*, 13(12): 5334–5355, 1993.

Dacey DM and Petersen MR. Dendritic field size and morphology of midget and parasol ganglion cells of the human retina. *Proceedings of the National Academy of Sciences of the United States of America*, 89(20): 9666–9670, 1992.

Damoiseaux JS, Rombouts SA, Barkhof F, Scheltens P, Stam CJ, Smith SM, et al. Consistent resting-state networks across healthy subjects. *Proceedings of the National Academy of Sciences of the United States of America*, 103(37): 13848–13853, 2006.

Danckert J and Goodale MA. Superior performance for visually guided pointing in the lower visual field. *Experimental Brain Research*, 137(3–4): 303–308, 2001.

Dauguet J, Peled S, Berezovskii V, and Delzescaux T. Comparison of fiber tracts derived from in-vivo DTI tractography with 3D histological neural tract. *NeuroImage*, 37(2): 530–538, 2007.

Deco G, Jirsa VK, and McIntosh AR. Emerging concepts for the dynamical organization of resting-state activity in the brain. *Nature Reviews Neuroscience*, 12(1): 43–56, 2011.

Dejerine J. *Anatomie des Centres Nerveux*. Paris: Rueff et Cie, 1895.

Dell'acqua F and Catani M. Structural human brain networks: Hot topics in diffusion tractography. *Current Opinion in Neurology*, 25(4): 375–383, 2012.

Dell'Acqua F, Coward J, Simmons A, Murphy DGM, Williams S, and Catani M. Mapping crossing fibres of the human brain

Please cite this article in press as: Thiebaut de Schotten M, et al., Subdivision of the occipital lobes: An anatomical and functional MRI connectivity study, Cortex (2012), http://dx.doi.org/10.1016/j.cortex.2012.12.007

with spherical deconvolution: Towards an atlas for clinico-anatomical correlation studies. *Proceedings of the International Society of Magnetic Resonance Medicine*, 17: 3562, 2009.

Dell'Acqua F, Rizzo G, Scifo P, Clarke RA, Scotti G, and Fazio F. A model-based deconvolution approach to solve fiber crossing in diffusion-weighted MR imaging. *IEEE Transactions on Biomedical Engineering*, 54(3): 462–472, 2007.

Dell'acqua F, Scifo P, Rizzo G, Catani M, Simmons A, Scotti G, et al. A modified damped Richardson-Lucy algorithm to reduce isotropic background effects in spherical deconvolution. *NeuroImage*, 49(2): 1446–1458, 2010.

Dell'Acqua F, Simmons A, Williams SCR, and Catani M. Can spherical deconvolution provide more information than fiber orientations? Hindrance modulated orientational anisotropy, a true-tract specific index to characterize white matter diffusion. *Human Brain Mapping*, 2012, http://dx.doi.org/10.1002/hbm.22080.

Epelbaum S, Pinel P, Gaillard R, Delmaire C, Perrin M, Dupont S, et al. Pure alexia as a disconnection syndrome: New diffusion imaging evidence for an old concept. *Cortex*, 44(8): 962–974, 2008.

Felleman DJ and Van Essen DC. Distributed hierarchical processing in the primate cerebral cortex. *Cerebral Cortex*, 1(1): 1–47, 1991.

Ferreira CT, Ceccaldi M, Giusiano B, and Poncet M. Separate visual pathways for perception of actions and objects: Evidence from a case of apperceptive agnosia. *Journal of Neurology, Neurosurgery, and Psychiatry*, 65(3): 382–385, 1998.

ffytche DH, Blom JD, and Catani M. Disorders of visual perception. *Journal of Neurology, Neurosurgery, and Psychiatry*, 81(11): 1280–1287, 2010.

Fischer E, Bülthoff Heinrich H, Logothetis NK, and Bartels A. Human areas V3A and V6 compensate for self-induced planar visual motion. *Neuron*, 73(6): 1228–1240, 2012.

Flechsig PE. *Anatomie des menschlichen Gehirns und Rückenmarks auf myelogenetischer Grundlage*. Leipzig: Thieme, 1920.

Fox MD, Corbetta M, Snyder AZ, Vincent JL, and Raichle ME. Spontaneous neuronal activity distinguishes human dorsal and ventral attention systems. *Proceedings of the National Academy of Sciences of the United States of America*, 103(26): 10046–10051, 2006.

Fox MD and Raichle ME. Spontaneous fluctuations in brain activity observed with functional magnetic resonance imaging. *Nature Reviews Neuroscience*, 8(9): 700–711, 2007.

Gaillard R, Naccache L, Pinel P, Clemenceau SP, Volle E, Hasboun D, et al. Direct intracranial, FMRI, and lesion evidence for the causal role of left inferotemporal cortex in reading. *Neuron*, 50(2): 191–204, 2006.

Gardner JL, Merriam EP, Movshon JA, and Heeger DJ. Maps of visual space in human occipital cortex are retinotopic, not spatiotopic. *Journal of Neuroscience*, 28(15): 3988–3999, 2008.

Gattass R, Nascimento-Silva S, Soares JG, Lima B, Jansen AK, Diogo AC, et al. Cortical visual areas in monkeys: Location, topography, connections, columns, plasticity and cortical dynamics. *Philosophical Transactions of the Royal Society of London. Series B, Biological Sciences*, 360(1456): 709–731, 2005.

Ginestet CE and Simmons A. Statistical parametric network analysis of functional connectivity dynamics during a working memory task. *NeuroImage*, 55(2): 688–704, 2010.

Greicius MD, Krasnow B, Reiss AL, and Menon V. Functional connectivity in the resting brain: A network analysis of the default mode hypothesis. *Proceedings of the National Academy of Sciences of the United States of America*, 100(1): 253–258, 2003.

Greicius MD, Supekar K, Menon V, and Dougherty RF. Resting-state functional connectivity reflects structural connectivity in the default mode network. *Cerebral Cortex*, 19(1): 72–78, 2009.

Grill-Spector K, Kushnir T, Hendler T, and Malach R. The dynamics of object-selective activation correlate with recognition performance in humans. *Nature Neuroscience*, 3(8): 837–843, 2000.

Hadjikhani N, Liu AK, Dale AM, Cavanagh P, and Tootell RB. Retinotopy and color sensitivity in human visual cortical area V8. *Nature Neuroscience*, 1(3): 235–241, 1998.

Hampson M, Driesen NR, Skudlarski P, Gore JC, and Constable RT. Brain connectivity related to working memory performance. *Journal of Neuroscience*, 26(51): 13338–13343, 2006.

He BJ, Snyder A, Vincent JL, Epstein A, Shulman GL, and Corbetta M. Breakdown of functional connectivity in frontoparietal networks underlies behavioral deficits in spatial neglect. *Neuron*, 53(6): 905–918, 2007.

Heilman KM and Van Den Abell T. Right hemisphere dominance for attention: The mechanism underlying hemispheric asymmetries of inattention (neglect). *Neurology*, 30(3): 327–330, 1980.

Holmes CJ, Hoge R, Collins L, Woods R, Toga AW, and Evans AC. Enhancement of MR images using registration for signal averaging. *Journal of Computer Assisted Tomography*, 22(2): 324–333, 1998.

Holmes GM. Disturbance of vision by cerebral lesions. *British Journal of Ophthalmology*, 2: 353–384, 1918.

Honey CJ, Sporns O, Cammoun L, Gigandet X, Thiran JP, Meuli R, et al. Predicting human resting-state functional connectivity from structural connectivity. *Proceedings of the National Academy of Sciences of the United States of America*, 106(6): 2035–2040, 2009.

Horton JC and Hoyt WF. Quadrantic visual field defects: A hallmark of lesions in extrastriate (V2/V3) cortex. *Brain*, 114: 1703–1718, 1991.

Hubel D and Wiesel T. Receptive fields, binocular interaction and functional architecture in the cat's visual cortex. *Journal of Physiology (London)*, 160: 106–154, 1962.

James TW, Humphrey GK, Gati JS, Menon RS, and Goodale MA. The effects of visual object priming on brain activation before and after recognition. *Current Biology*, 10(17): 1017–1024, 2000.

Jbabdi S and Behrens TEJ. Specialization: The connections have it. *Nature Neuroscience*, 15(2): 171–172, 2012.

Jbabdi S, Woolrich MW, and Behrens TE. Multiple-subjects connectivity-based parcellation using hierarchical Dirichlet process mixture models. *NeuroImage*, 44(2): 373–384, 2009.

Jenkinson M, Bannister P, Brady M, and Smith S. Improved optimization for the robust and accurate linear registration and motion correction of brain images. *NeuroImage*, 17(2): 825–841, 2002.

Jenkinson M and Smith S. A global optimisation method for robust affine registration of brain images. *Medical Image Analysis*, 5(2): 143–156, 2001.

Jewell G and McCourt ME. Pseudoneglect: A review and meta-analysis of performance factors in line bisection tasks. *Neuropsychologia*, 38(1): 93–110, 2000.

Johansen-Berg H, Behrens TEJ, Robson MD, Drobnjak I, Rushworth MFS, Brady JM, et al. Changes in connectivity profiles define functionally distinct regions in human medial frontal cortex. *Proceedings of the National Academy of Sciences of the United States of America*, 101(36): 13335–13340, 2004.

Jones DK. Studying connections in the living human brain with diffusion MRI. *Cortex*, 44(8): 936–952, 2008.

Jones DK. Challenges and limitations of quantifying brain connectivity in vivo with diffusion MRI. *Imaging in Medicine*, 2(3): 341–355, 2010.

Jones DK, Williams SC, Gasston D, Horsfield MA, Simmons A, and Howard R. Isotropic resolution diffusion tensor imaging with whole brain acquisition in a clinically acceptable time. *Human Brain Mapping*, 15(4): 216–230, 2002.

Kiviniemi V, Kantola JH, Jauhiainen J, Hyvarinen A, and Tervonen O. Independent component analysis of nondeterministic fMRI signal sources. *NeuroImage*, 19(2 Pt 1): 253–260, 2003.

Klein A, Andersson J, Ardekani BA, Ashburner J, Avants B, Chiang MC, et al. Evaluation of 14 nonlinear deformation

algorithms applied to human brain MRI registration. *NeuroImage*, 46(3): 786–802, 2009.
Kleinschmidt A and Cohen L. The neural bases of prosopagnosia and pure alexia: Recent insights from functional neuroimaging. *Current Opinion in Neurology*, 19(4): 386–391, 2006.
Kourtzi Z and Kanwisher N. Cortical regions involved in perceiving object shape. *Journal of Neuroscience*, 20(9): 3310–3318, 2000.
Kraft A, Grimsen C, Kehrer S, Spang K, Bahnemann M, Prass M, et al. Neurological- and neuropsychological characteristics of occipital, occipital-temporal and occipital-parietal infarction. *Cortex*, this issue.
Kraft A, Pape N, Hagendorf H, Schmidt S, Naito A, and Brandt SA. What determines sustained visual attention? The impact of distracter positions, task difficulty and visual fields compared. *Brain Research*, 1133(1): 123–135, 2007.
Kravitz DJ, Saleem KS, Baker CI, and Mishkin M. A new neural framework for visuospatial processing. *Nature Reviews Neuroscience*, 12(4): 217–230, 2011.
Kujovic M, Zilles K, Malikovic A, Schleicher A, Mohlberg H, Rottschy C, et al. Cytoarchitectonic mapping of the human dorsal extrastriate cortex. *Brain Structure and Function*, 2012, http://dx.doi.org/10.1007/s00429-012-0390-9.
Lawes INC, Barrick TR, Murugam V, Spierings N, Evans DR, Song M, et al. Atlas-based segmentation of white matter tracts of the human brain using diffusion tensor tractography and comparison with classical dissection. *NeuroImage*, 39(1): 62–79, 2008.
Leventhal AG, Rodieck RW, and Dreher B. Central projections of cat retinal ganglion cells. *Journal of Comparative Neurology*, 237(2): 216–226, 1985.
Levine MW and McAnany JJ. The relative capabilities of the upper and lower visual hemifields. *Vision Research*, 45(21): 2820–2830, 2005.
Malikovic A, Amunts K, Schleicher A, Mohlberg H, Eickhoff SB, Wilms M, et al. Cytoarchitectonic analysis of the human extrastriate cortex in the region of V5/MT+: A probabilistic, stereotaxic map of area hOc5. *Cerebral Cortex*, 17(3): 562–574, 2007.
Mantini D, Perrucci MG, Del Gratta C, Romani GL, and Corbetta M. Electrophysiological signatures of resting state networks in the human brain. *Proceedings of the National Academy of Sciences of the United States of America*, 104(32): 13170–13175, 2007.
Mars RB, Jbabdi S, Sallet J, O'Reilly JX, Croxson PL, Olivier E, et al. Diffusion-weighted imaging tractography-based parcellation of the human parietal cortex and comparison with human and macaque resting-state functional connectivity. *Journal of Neuroscience*, 31(11): 4087–4100, 2011.
McAvoy M, Larson-Prior L, Nolan TS, Vaishnavi SN, Raichle ME, and d'Avossa G. Resting states affect spontaneous BOLD oscillations in sensory and paralimbic cortex. *Journal of Neurophysiology*, 100(2): 922–931, 2008.
Meissirel C, Wikler KC, Chalupa LM, and Rakic P. Early divergence of magnocellular and parvocellular functional subsystems in the embryonic primate visual system. *Proceedings of the National Academy of Sciences of the United States of America*, 94(11): 5900–5905, 1997.
Mesulam MM. Imaging connectivity in the human cerebral cortex: The next frontier? *Annals of Neurology*, 57(1): 5–7, 2005.
Moseley ME, Cohen Y, Kucharczyk J, Mintorovitch J, Asgari HS, Wendland MF, et al. Diffusion-weighted MR imaging of anisotropic water diffusion in cat central nervous system. *Radiology*, 176(2): 439–445, 1990.
Niebauer CL and Christman SD. Upper and lower visual field differences in categorical and coordinate judgments. *Psychonomic Bulletin and Review*, 5(1): 147–151, 1998.
Petrides M and Pandya DN. Distinct parietal and temporal pathways to the homologues of Broca's area in the monkey. *Public Library of Sciences Biology*, 7(8): e1000170, 2009.
Pisella L, Binkofski F, Lasek K, Toni I, and Rossetti Y. No double-dissociation between optic ataxia and visual agnosia: Multiple sub-streams for multiple visuo-manual integrations. *Neuropsychologia*, 44(13): 2734–2748, 2006.
Pisella L, Sergio L, Blangero A, Torchin H, Vighetto A, and Rossetti Y. Optic ataxia and the function of the dorsal stream: Contributions to perception and action. *Neuropsychologia*, 47(14): 3033–3044, 2009.
Previc FH. Functional specialization in the lower and upper visual-fields in humans – Its ecological origins and neurophysiological implications. *Behavioral and Brain Sciences*, 13(3): 519–541, 1990.
Raichle ME, MacLeod AM, Snyder AZ, Powers WJ, Gusnard DA, and Shulman GL. A default mode of brain function. *Proceedings of the National Academy of Sciences of the United States of America*, 98(2): 676–682, 2001.
Raichle ME and Snyder AZ. A default mode of brain function: A brief history of an evolving idea. *NeuroImage*, 37(4): 1083–1090. discussion 1097–1089, 2007.
Riddoch MJ and Humphreys GW. A case of integrative visual agnosia. *Brain*, 110(Pt 6): 1431–1462, 1987.
Riddoch MJ, Humphreys GW, Akhtar N, Allen H, Bracewell RM, and Schofield AJ. A tale of two agnosias: Distinctions between form and integrative agnosia. *Cognitive Neuropsychology*, 25(1): 56–92, 2008.
Rilling JK, Glasser MF, Preuss TM, Ma X, Zhao T, Hu X, et al. The evolution of the arcuate fasciculus revealed with comparative DTI. *Nature Neuroscience*, 11(4): 426–428, 2008.
Rizzo M, Nawrot M, and Zihl J. Motion and shape perception in cerebral akinetopsia. *Brain*, 118(Pt 5): 1105–1127, 1995.
Rottschy C, Eickhoff SB, Schleicher A, Mohlberg H, Kujovic M, Zilles K, et al. Ventral visual cortex in humans: Cytoarchitectonic mapping of two extrastriate areas. *Human Brain Mapping*, 28(10): 1045–1059, 2007.
Seeley WW, Menon V, Schatzberg AF, Keller J, Glover GH, Kenna H, et al. Dissociable intrinsic connectivity networks for salience processing and executive control. *Journal of Neuroscience*, 27(9): 2349–2356, 2007.
Sergent J, Ohta S, and MacDonald B. Functional neuroanatomy of face and object processing. A positron emission tomography study. *Brain*, 115(Pt 1): 15–36, 1992.
Skudlarski P, Jagannathan K, Calhoun VD, Hampson M, Skudlarska BA, and Pearlson G. Measuring brain connectivity: Diffusion tensor imaging validates resting state temporal correlations. *NeuroImage*, 43(3): 554–561, 2008.
Smith GE. A new topographical survey of human cerebral cortex. *Journal of Anatomy*, 41: 237–254, 1907.
Smith S. *Resting-state Signals: Identification, Classification & Relation to Brain Connectivity*. Montreal, Quebec: International Society for Magnetic Resonance in Medicine, 2011.
Smith SM. Fast robust automated brain extraction. *Human Brain Mapping*, 17(3): 143–155, 2002.
Smith SM, Fox PT, Miller KL, Glahn DC, Fox PM, Mackay CE, et al. Correspondence of the brain's functional architecture during activation and rest. *Proceedings of the National Academy of Sciences of the United States of America*, 106(31): 13040–13045, 2009.
Smith SM, Jenkinson M, Woolrich MW, Beckmann CF, Behrens TEJ, Johansen-Berg H, et al. Advances in functional and structural MR image analysis and implementation as FSL. *NeuroImage*, 23(Suppl. 1): S208–S219, 2004.
Thiebaut de Schotten M, Dell'Acqua F, Forkel SJ, Simmons A, Vergani F, Murphy DGM, et al. A lateralized brain network for visuospatial attention. *Nature Neuroscience*, 14(10): 1245–1246, 2011a.

Please cite this article in press as: Thiebaut de Schotten M, et al., Subdivision of the occipital lobes: An anatomical and functional MRI connectivity study, Cortex (2012), http://dx.doi.org/10.1016/j.cortex.2012.12.007

Thiebaut de Schotten M, Dell'acqua F, Valabregue R, and Catani M. Monkey to human comparative anatomy of the frontal lobe association tracts. *Cortex*, 48: 82–96, 2012.

Thiebaut de Schotten M, Ffytche DH, Bizzi A, Dell'Acqua F, Allin M, Walshe M, et al. Atlasing location, asymmetry and inter-subject variability of white matter tracts in the human brain with MR diffusion tractography. *NeuroImage*, 54(1): 49–59, 2011b.

Tootell RB, Hadjikhani NK, Mendola JD, Marrett S, and Dale AM. From retinotopy to recognition: fMRI in human visual cortex. *Trends in Cognitive Sciences*, 2(5): 174–183, 1998.

Tootell RB, Mendola JD, Hadjikhani NK, Ledden PJ, Liu AK, Reppas JB, et al. Functional analysis of V3A and related areas in human visual cortex. *Journal of Neuroscience*, 17(18): 7060–7078, 1997.

Turner R, Le Bihan D, Maier J, Vavrek R, Hedges LK, and Pekar J. Echo-planar imaging of intravoxel incoherent motion. *Radiology*, 177(2): 407–414, 1990.

Ungerleider LG and Desimone R. Projections to the superior temporal sulcus from the central and peripheral field representations of V1 and V2. *Journal of Comparative Neurology*, 248(2): 147–163, 1986.

Ungerleider LG and Mishkin M. Two cortical visual systems. In Ingle DJ, Goodale MA, and Mansfield RJW (Eds), *Analysis of Visual Behavior*. Boston: MIT Press, 1982.

Van Essen DC. Organization of visual areas in macaque and human cerebral cortex. In Chalupa L and Werner J (Eds), *The Visual Neurosciences*. Bradford: MIT Press, 2003: 507.

Van Essen DC and Maunsell JHR. Hierarchical organization and functional streams in the visual cortex. *Trends in Neurosciences*, 6: 370–375, 1983.

Van Essen DC, Newsome JHR, and Bixby JL. The projections from striate cortex (V1) to areas V2 and V3 in the Macaque monkey: Asymmetries, areal boundaries, and patchy connections. *Journal of Comparative Neurology*, 224: 451–480, 1986.

Van Essen DC, Newsome WT, and Bixby JL. The pattern of interhemispheric connections and its relationship to extrastriate visual areas in the macaque monkey. *Journal of Neuroscience*, 2(3): 265–283, 1982.

Vergani F, Mahmood S, Morris C, Mitchell P, and Catani M. Intralobar fibres of the iccipital lobe: a post mortem dissection study. *Cortex*, this issue.

Verrey L. Hémiachromatopsie droite absolue. Conservation partielle de la perception lumineuse et des formes. Ancien kyste hémorrhagique de la partie inférieure du lobe occipital gauche. *Archives of Ophthalmology (Paris)*, 8: 289–300, 1888.

Vogt C and Vogt O. Ergebnisse unserer hirnforschung. *Journal of Psychology and Neurology*, 25: 279–461, 1919.

Von Economo C and Koskinas GN. *Die Cytoarchitektonik der Hirnrinde des erwachsenen Menschen*. Berlin: Springer-Verlag, 1925.

Warrington EK and James M. Visual apperceptive agnosia: A clinico-anatomical study of three cases. *Cortex*, 24(1): 13–32, 1988.

Wilson JR. Circuitry of the dorsal lateral geniculate nucleus in the cat and monkey. *Acta Anatomica*, 147(1): 1–13, 1993.

Yeterian EH and Pandya DN. Fiber pathways and cortical connections of preoccipital areas in rhesus monkeys. *Journal of Comparative Neurology*, 518(18): 3725–3751, 2010.

Zeki S. Cerebral akinetopsia (visual motion blindness). A review. *Brain*, 114(Pt 2): 811–824, 1991.

Zhang Y, Brady M, and Smith SM. Segmentation of brain MR images through a hidden Markov random field model and the expectation-maximization algorithm. *IEEE Transaction in Medical Imaging*, 20: 45–57, 2001.

Zhou J, Liu X, Song W, Yang Y, Zhao Z, Ling F, et al. Specific and nonspecific thalamocortical functional connectivity in normal and vegetative states. *Consciousness and Cognition*, 20(2): 257–268, 2011.

Zilles K and Clarke S. Architecture, connectivity, and transmitter receptors of human extrastriate visual cortex. In Rockland KKJ and Peters A (Eds), *Cerebral Cortex*. Extrastriate Cortex in Primates. New York: Plenum Press, 1997: 673–742.

Zilles K and Schleicher A. Cyto- and myeloarchitecture of human visual cortex and periodical GABAA receptor distribution. In Gulyas B, Ottoson D, and Roland P (Eds), *Functional Organization of the Human Visual Cortex*. Oxford: Pergamon Press, 1993.

Zilles K, Werners R, Busching U, and Schleicher A. Ontogenesis of the laminar structure in areas 17 and 18 of the human visual cortex. A quantitative study. *Anatomy and Embryology*, 174(3): 339–353, 1986.

Zou H, Hastie T, and Tibshirani R. Sparse principal component analysis. *Journal of Computational and Graphical Statistics*, 15(2): 265–286, 2006.

Please cite this article in press as: Thiebaut de Schotten M, et al., Subdivision of the occipital lobes: An anatomical and functional MRI connectivity study, Cortex (2012), http://dx.doi.org/10.1016/j.cortex.2012.12.007